1999

On the joint estimation of model and satellite sea surface height anomaly errors

Tokmakian, R.

Ocean Modeling, Volume 1, pp. 39-52, 1999.
http://hdl.handle.net/10945/43120

PERGAMON

Ocean Modelling 1 (1999) 39–52

Ocean Modelling

On the joint estimation of model and satellite sea surface height anomaly errors

R. Tokmakian [a,*], P.G. Challenor [b]

[a] *Department of Oceanography, Naval Postgraduate School, Monterey, CA 93943-5122, USA*
[b] *James Rennell Division for Ocean Circulation and Climate, Southampton Oceanography Centre, Southampton, UK*

Abstract

We describe a technique to estimate the error field in the sea surface height (SSH) anomaly field of an ocean model through the joint use of SSH anomaly fields measured from two satellites, Topex/Poseidon (T/P) and ERS-2. The joint error maps for the model, T/P and ERS-2 show distributions distinctly different from one another and globally inhomogeneous. Both sampling errors and instrument errors are represented in the mapped fields. Additionally, we compare the joint error estimation method to a technique using the model and only one satellite, and show the importance of the cross covariance between the measured SSH and the true SSH field in the estimation of the error field. Finally, we look at the distribution of the error versus the variance of the SSH at a location. This logged distribution suggests that the model errors are generally proportional to the model's variance (regression coefficient of 0.99, globally) while the satellites' errors do not exhibit this linear relationship (regression coefficients on the average of 0.60). The comparison of the two satellite distributions implies that ERS-2 has a lower sampling error than the T/P instrument except in the tropical region.

Keywords: Modelling; Models; Ocean circulation; Altimetry; Sea level variations

1. Introduction

Over recent years there has been an increased emphasis in oceanographic research on the assimilation of data into ocean models. The more sophisticated methods (for example, Kalman filters or adjoint methods) require that error fields be specified for both the observational data that are to be incorporated into the model and for the model itself. Errors can be specified for observational quantities because there is usually some knowledge of the measurement errors intrinsic

* Corresponding author. Tel.: +1-831-656-3255; fax: +1-831-656-2712.
E-mail address: robint@ucar.edu (R. Tokmakian)

1463-5003/99/$ - see front matter
PII: S1463-5003(99)00006-2

to the instrument. In contrast, model error is difficult, if not impossible to define. This paper describes a technique that can be used to estimate simultaneously model and data error.

2. Model and data description

This paper attempts to find the errors associated with the sea surface height (SSH) variability field in both a model and associated altimeter data. The model used is the Semtner/Chervin Parallel Ocean Climate Model, version POCM 4C. This model incorporates daily varying surface fluxes of momentum, heat, and freshwater over a period of 19 years from 1979 to 1997. The basic formulation of the model is given in Semtner et al. (1992) and Stammer et al. (1996). The fluxes used to force this simulation are computed from the ECMWF reanalysis data set for the period of 1979 to 1993; after which the operational fields from ECMWF are used for the forcing (1994–present). The model also has a free surface (Killworth et al., 1991). For this paper, only model output which coincides with the time period when we have data from both satellites will be used (May 1995 to 1997) and all the references to SSH refer to SSH anomaly fields. The model resolution is at an average of 1/4° and is on a Mercator grid. For the analysis below, the model SSH (with a five-year mean removed) has been binned into $2^\circ \times 2^\circ$ bins at its temporal sampling period of every three days (three-dimensional fields of u, v, t, s and SSH are averaged and saved every three days during the simulation). These binned, three-day averaged fields are then interpolated to the monthly sampling (35-day) of ERS-2 using linear interpolation. In other words, we are subsampling the model fields to the mid point of the ERS-2 repeat 35-day sampling period.

Researchers are very fortunate to have multiple satellite altimeters sampling the sea surface of the ocean during the same period with different temporal and spatial sampling characteristics. We use data from two of these altimeters to estimate joint model, ERS-2 and Topex/Poseidon (T/P) errors. The processed satellite data for both ERS-2 and T/P are from the NASA Pathfinder data set (Koblinsky, 1998). The SSHs have been specified at one second intervals along a reference track referenced to a mean sea surface. The T/P SSHs were computed using the JGM3 orbits (Marshall et al., 1995). The ERS-2 orbit correction is computed using the DGM-E04 gravity model (Scharroo and Visser, 1998). The geophysical corrections: solid earth body tide, pole tide, load tide, ocean tide, cross-track geoid correction, and em-bias corrections are the same for both satellite data sets (ocean and load corrections: Schramma and Ray, 1994, pole and solid earth tide: TOPEX SWT algorithms, em-bias: Gaspar and Ogor, 1996). The wet tropospheric, dry tropospheric (and related inverse barometer), and ionospheric corrections differ between the satellite data sets. The wet tropospheric correction on both the satellites is based on their individual on board radiometer, each with its own unique error characteristics. The ionospheric correction for T/P is based upon measurements from its dual frequency altimeter while on ERS-2, the correction is based on a model (IRI95 version 13, Bilitza, 1997). The dry tropospheric correction for T/P and ERS-2 are calculated using information from meteorological models (NCEP and ECMWF, respectively). An oscillator drift correction is also applied to T/P (Hancock and Haynes, 1996).

We have gridded each data set (ERS-2 and T/P) into $2^\circ \times 2^\circ$ bins at their repeat track frequency. The T/P data are linearly interpolated to the monthly (35-day) sampling of ERS2. Each realization of SSH, (model, T/P, and ERS-2 fields), is sampling somewhat different portions of the total spectrum of the true SSH. When gridded and interpolated to the same spatial and temporal

grid, the "monthly" maps will contain errors. These errors are what we are partially determining in this paper. The model SSH is on a regular Mercator grid with the temporal averages every three days; the T/P field is sampled every 10 days with a track separation of 300 km at the equator progressing to shorter separations at higher latitudes; and ERS-2 has a 35-day repeat with equator track separation around 60 km. Because of these different samplings, the three sets of observations and simulation fields could be averaged, binned, interpolated in a variety of ways. If the fields were averaged into two degree fields by month, the result would be somewhat different.

3. Error calculation and results of application

To examine the problem of model error, we will use these three estimates of SSH variability, that from an ocean model forced with realistic winds, from the 10-day repeating T/P altimeter, and from the 35-day repeating altimeter ERS-2. Each measures the variability of SSH and each also has some error in its own measurement. We begin by defining the signal and its error for each measurement. We have

$$sm = h + em, \tag{1}$$

$$st = h + et \tag{2}$$

and

$$se = h + ee, \tag{3}$$

where sm, st, and se are the computed or measured values of SSH for the model, T/P, and ERS-2, respectively; em, et, and ee are their associated errors, and h is the true ocean SSH anomaly signal. $E(em^2)$, $E(et^2)$ and $E(ee^2)$ are the mean square errors (MSE) for the model, T/P and ERS-2 respectively. We must note that we assume the use of expectation operators for the true sea surface is well defined. In this paper we are working with altimetry and in the absence of an independent geoid we have to work with anomalies. Thus,

$$E(sm) = E(st) = E(se) = E(h) = 0 \tag{4}$$

and we can say nothing about any bias. Returning to the MSE we have from (1)–(3)

$$E(sm^2) = E(h^2) + 2E(em \cdot h) + E(em^2), \tag{5}$$

$$E(st^2) = E(h^2) + 2E(et \cdot h) + E(et^2) \tag{6}$$

and

$$E(se^2) = E(h^2) + 2E(ee \cdot h) + E(ee^2), \tag{7}$$

$E(em^2)$, $E(et^2)$ and $E(ee^2)$ are the unknowns which we are trying to determine. The expected values of the cross-products (covariances) are given by:

$$E(st \cdot sm) = E(h^2) + E(h \cdot et) + E(h \cdot em) + E(et \cdot em), \tag{8}$$

$$E(se \cdot sm) = E(h^2) + E(h \cdot ee) + E(h \cdot em) + E(ee \cdot em), \tag{9}$$

and

$$E(st \cdot se) = E(h^2) + E(h \cdot et) + E(h \cdot ee) + E(et \cdot ee). \tag{10}$$

We have confidence that the errors between the model and either satellite instrument are independent, allowing for the elimination of $E(et \cdot em)$ and $E(ee \cdot em)$. Using Eqs. (8)–(10) to eliminate the variance of the true SSH, h, and its covariance with the error terms ($E(h^2)$, $E(h \cdot em)$, $E(h \cdot et)$, and $E(h \cdot ee)$), we find that the error variances can be now be written in terms that can be calculated with the exception of $E(et \cdot ee)$:

$$E(em^2) + E(et \cdot ee) = E(sm^2) - E(st \cdot sm) + E(st \cdot se) - E(sm \cdot se), \tag{11}$$

$$E(et^2) - E(et \cdot ee) = E(st^2) - E(st \cdot sm) - E(st \cdot se) + E(sm \cdot se), \tag{12}$$

and

$$E(ee^2) - E(et \cdot ee) = E(se^2) + E(st \cdot sm) - E(st \cdot se) - E(sm \cdot se). \tag{13}$$

The term, $E(et \cdot ee)$, the covariance between the errors in the corrections applied to the T/P and ERS-2 data requires more thought on how to estimate its size. $E(et \cdot ee)$ can be expanded to be equal to the sum of the covariance of the individual corrections

$$E(et \cdot ee)_{\text{total}} = E(et \cdot ee)_{\text{ib}} + E(et \cdot ee)_{\text{tide}} + E(et \cdot ee)_{\text{em}} + \text{other small terms}, \tag{14}$$

where ib relates to the inverse barometer (IB) correction, em relates to the em-bias correction, and tide relates to the tidal correction. All the other errors associated with the term $E(et \cdot ee)$ are orders of magnitude smaller and we ignore them. Each term on the right-hand side of Eq. (14) can be estimated by the following method. For simplicity, we describe only how to estimate $E(et \cdot ee)_{\text{ib}}$. We compute $E(ee^2)$, $E(et^2)$, and $E(em^2)$ in the case where we apply the IB correction to the T/P data (case A) and in the case where we do not (case B). Note, for both cases, the IB correction is applied to the ERS-2 data. This gives us two estimates of the ERS-2 error: $E(ee^2)_{\text{A}}$ and $E(ee^2)_{\text{B}}$. It can also be shown, using Eqs. (5)–(10) and defining st for case B as: $st = h + et + I$, where I represents the neglected IB correction, that the difference

$$E(ee^2)_{\text{A}} - E(ee^2)_{\text{B}} = E(et \cdot ee)_{\text{ib}} + E(I \cdot ee), \tag{15}$$

where $E(I \cdot ee)$ represents a new term which correlates the IB correction itself with the IB error within the ERS-2 data set. This second part is much larger than the term we are actually interested in: $E(et \cdot ee)_{\text{ib}}$. We calculate the ratio of the added error contribution to $E(et^2)$ (from neglecting to include the IB correction in the T/P data) to the variance of the IB correction itself. Assuming a linear relationship between the IB correction and its error, we use the ratio to estimate the percentage of $[E(et \cdot ee)_{\text{ib}} + E(I \cdot ee)]$ associated with $E(I \cdot ee)$. The result is that a large portion of the difference in Eq. (15) is attributable to the $E(I \cdot ee)$ term. By removing this percentage from the difference, we get an estimate of $E(et \cdot ee)_{\text{ib}}$ which is shown in Fig. 1(c). A similar exercise is performed using the tide correction and em-bias correction, resulting in maps shown in Figs. 1(a) and (b). It is easily seen that the covariance of the errors are quite small (most less than 2 cm^2) over most of the ocean. The maximum covariance associated with the tidal error is about 2 cm. The covariance for the em-bias error is also of the order 2–3 cm (Gaspar and Ogor, 1996), with the highest covariances at mid to high latitudes. The em-bias

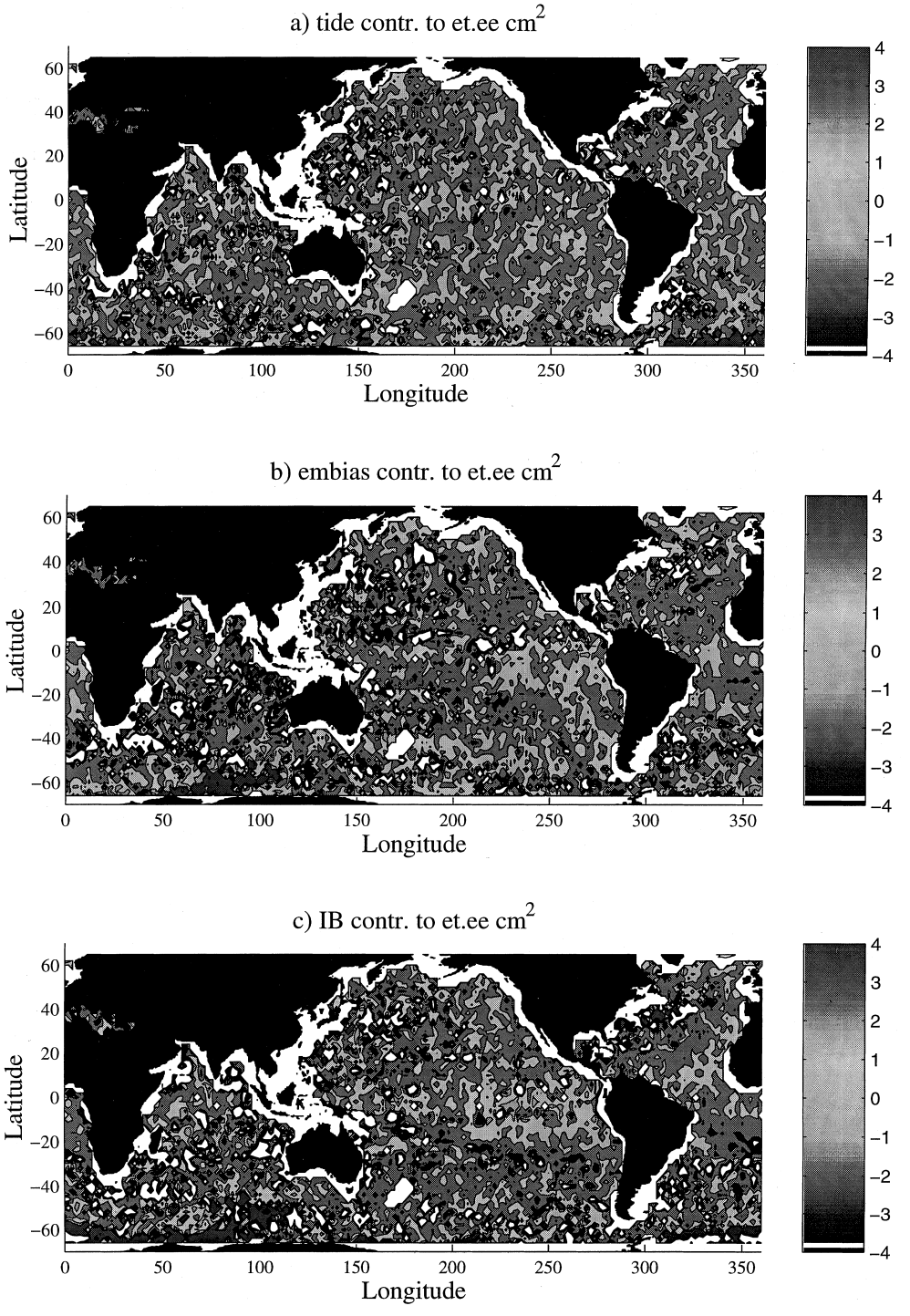

Fig. 1. (a) Global estimated error $E(et \cdot ee)_{\text{tide}}$, (b) global estimated error $E(et \cdot ee)_{\text{embias}}$, (c) global estimated error $E(et \cdot ee)_{\text{ib}}$. Units are in cm^2.

correction is related to significant wave height and waves are larger at the higher latitudes. In the tropics, we know that the IB correction is in error (Fu and Pihos, 1994). The size of the IB correction in these regions is small (1–2 cm).

We add (Eqs. (12) and (13)) or remove (Eq. (11)) the sum of the maps in Fig. 1 to those computed with Eqs. (11)–(13), which results in the "error fields" for our coincident model fields and data, seen in Fig. 2. Fig. 2(a) is the model error field, (b) and (c) are the error fields for T/P and ERS-2, respectively. The values in the plots are the square roots of $E(et^2)$, $E(ee^2)$, and $E(em^2)$. The maximum values of the square root of $E(em^2)$ is 35.78 cm, of $E(et^2)$, 31.65 cm, and for $E(ee^2)$ 46.85 cm. The means of the three fields are 5.33, 3.65, and 4.08 cm, respectively.

3.1. Error fields for the two satellites

We first examine the error fields of the two satellite pictures (Figs. 2(b) and (c)). It is clear on the scale of 2° resolution and at one month, the two satellites have low errors over much of the ocean and thus, will produce a similar representation of SSH variability. For the most part, the errors are within the 2–4 cm accuracy quoted for the satellite measurements. The black areas are land, the white areas around the edges are relatively shallow areas (including the area around New Zealand) where the altimeter signal has not been used. The other white areas visible in Fig. 2(b) in the tropical eastern Pacific are areas of negative error variance, we believe that these are related to the incorrect use of the inverse barometer correction, see above. Along the southern boundary of the ERS-2 error map (Fig. 2(c)), large errors exist due to unflagged SSH anomalies contaminated with ice in the Pathfinder data set. Ideally, these points could be removed before further use of the SSH fields themselves. Here, the contaminated data show how the satellite error maps do identify errors in the SSH fields. Seasonal plots of the ERS-2 SSH variability clearly show that this southern region is ice contaminated when a qualitative comparison is performed with seasonal observational ice maps which show winter ice patterns extending to around 60°S in the Atlantic sector and to only about 70°S in the Indian and Pacific sectors. Comparing the two error maps, the mesoscale related errors are reduced in the ERS-2 map (Fig. 2(c)) as compared to the T/P map (Fig. 2(b)). This can be seen in the highly energetic regions of the Gulf Stream, the Kuroshio, the Agulhas retroflection and eddy path into the South Atlantic, and the Brazil Confluence. Due to the finer spatial sampling of the ERS-2 instrument over that of the T/P, ERS-2 has a lower error field than T/P in these regions. Similarly, because of its temporal sampling characteristic (10 days), the T/P instrument has lower errors in the tropical region and is better at sampling the fast moving Kelvin waves. The errors in the Southern ocean are very similar (disregarding the very southern portion in the ERS map) because the T/P sampling is able to resolve, spatially, much smaller features at these latitudes. The fact that the data from the two satellites are producing similar views of the ocean can be confirmed by computing a map of correlation between the two sensors' measurements.

3.2. Model error field

Fig. 2(a) shows an estimate of the model error. As one might expect, the amplitude of the errors are much larger for the model than the errors calculated for either of the satellite measured data. From other analyses (Stammer et al., 1996; Tokmakian, 1996), we know that the model's energy is

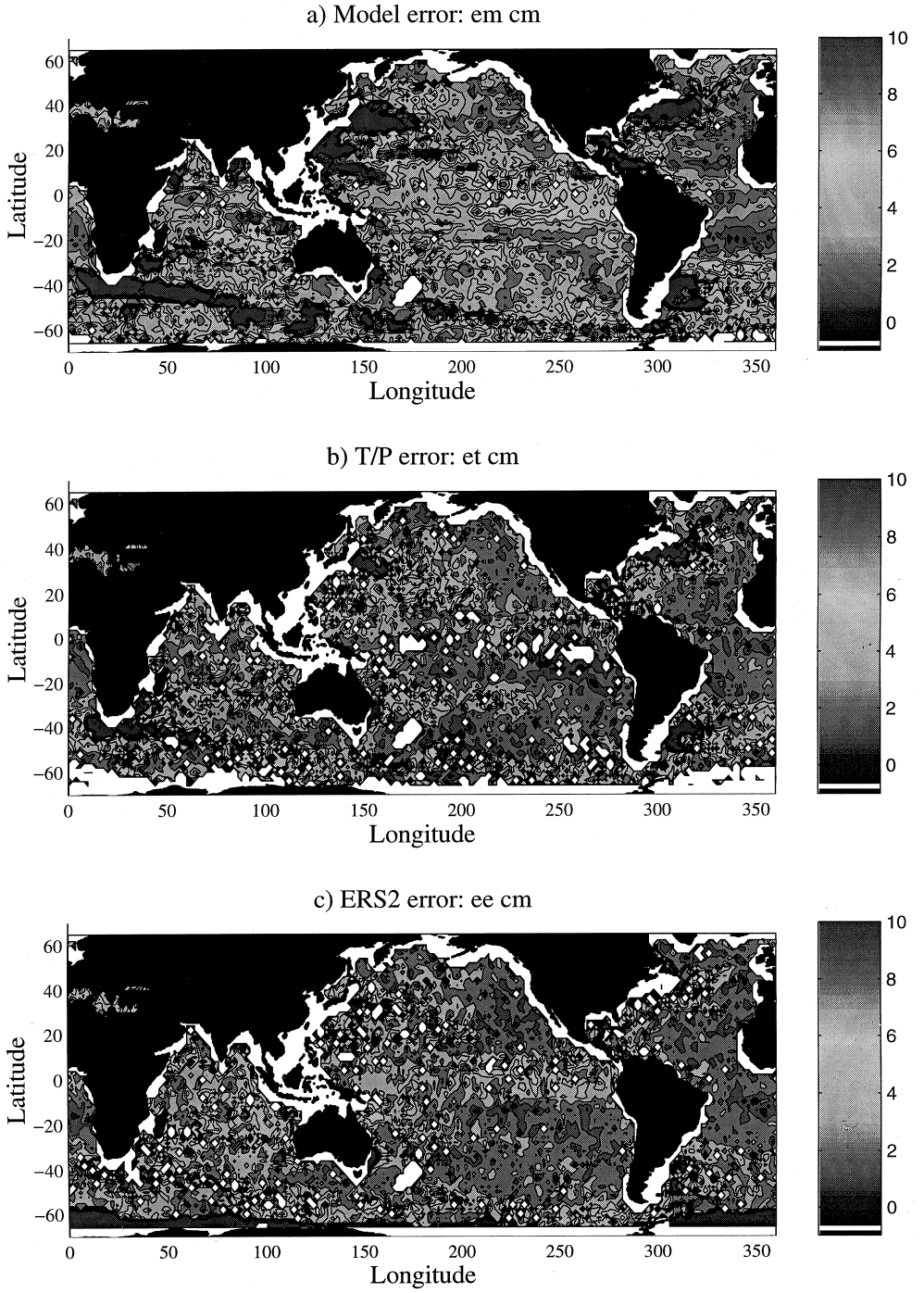

Fig. 2. (a) Global estimated error field for POCM 4C SSH anomaly field, (b) global estimated error field for T/P, (c) global estimated error field for ERS-2. Units are in cm^2. White denotes a negative estimate.

low for the eddy rich areas and this corresponds to the error map's high values in these regions (Southern Ocean, Kuroshio, Gulf Stream and Brazil Confluence).

In other regions, such as around 20°N, we have other evidence that the model does not produce a realistic simulation. Fig. 3 shows a map of correlations of the model's SSH signal with the University of Hawaii Sea Level Center's global tide gauge data set (Kilonsky and Caldwell, 1991). This data set consists of daily measurements of sea level taken over long periods of time (some stations begin prior to 1979, the beginning of the model simulation) and the comparison of the model to the data reflects the realism of the model at various frequencies. For this comparison, the model data was processed as in Tokmakian (1996). The low correlations in the North Pacific around a latitude of 20°N correspond to a similar area in the error map (Fig. 2(a)) which has high values.

3.3. Comparison to another technique

Other researchers have used methods to determine model and satellite errors using only two sources: a model and a single satellite (e.g. Fukumori, 1995). This limits the equations to three (Eqs. (5), (6) and (8)). If we set all the cross-products (covariances) to zero, from Eq. (8) we get

$$E(st \cdot sm) = E(h^2). \tag{16}$$

Substituting this back into Eqs. (5) and (6) gives

$$E(em^2) = E(sm^2) - E(st \cdot sm) \tag{17}$$

and

$$E(et^2) = E(st^2) - E(st \cdot sm). \tag{18}$$

This introduces some questions about how reasonable it is to ignore all the cross-products in the equations. Not only are $E(em \cdot et)$, $E(em \cdot ee)$, and $E(ee \cdot et)$ set to zero, but the other cross terms are as well, $E(h \cdot et)$, $E(h \cdot em)$, and $E(h \cdot ee)$. In other words, unlike the method proposed earlier in the paper we are ignoring the covariance between the true SSH (h) and specific error of the instrument (model or satellite), which includes the "null" space of the instrument, which is not represented or sampled. By looking at the differences between the variance error estimate computed in Section 3.1 (which does not assume that $E(h \cdot et)$, $E(h \cdot em)$, and $E(h \cdot ee)$ are zero) and estimates from the formulae in this section, we can assess how large these covariances are.

Given the T/P data and the model output we can produce an error estimate for T/P from Eq. (18). Alternatively we can consider the two satellite data sets and produce another estimate of the T/P error

$$E(et^2) = E(st^2) - E(st \cdot se). \tag{19}$$

Fig. 4 (Eqs. (18) and (19)) shows the two estimates of "error" in T/P. Similar figures can be created for the "error" in ERS-2 and the model. Each of the two estimates should produce a similar image of the extent of the T/P error field, but they do not because the assumption is made that $E(h \cdot et) = E(h \cdot ee) = E(h \cdot em) = 0$. Note, the white areas in the tropical Pacific are regions where we have not accounted for all the error, and the computation results in a negative error

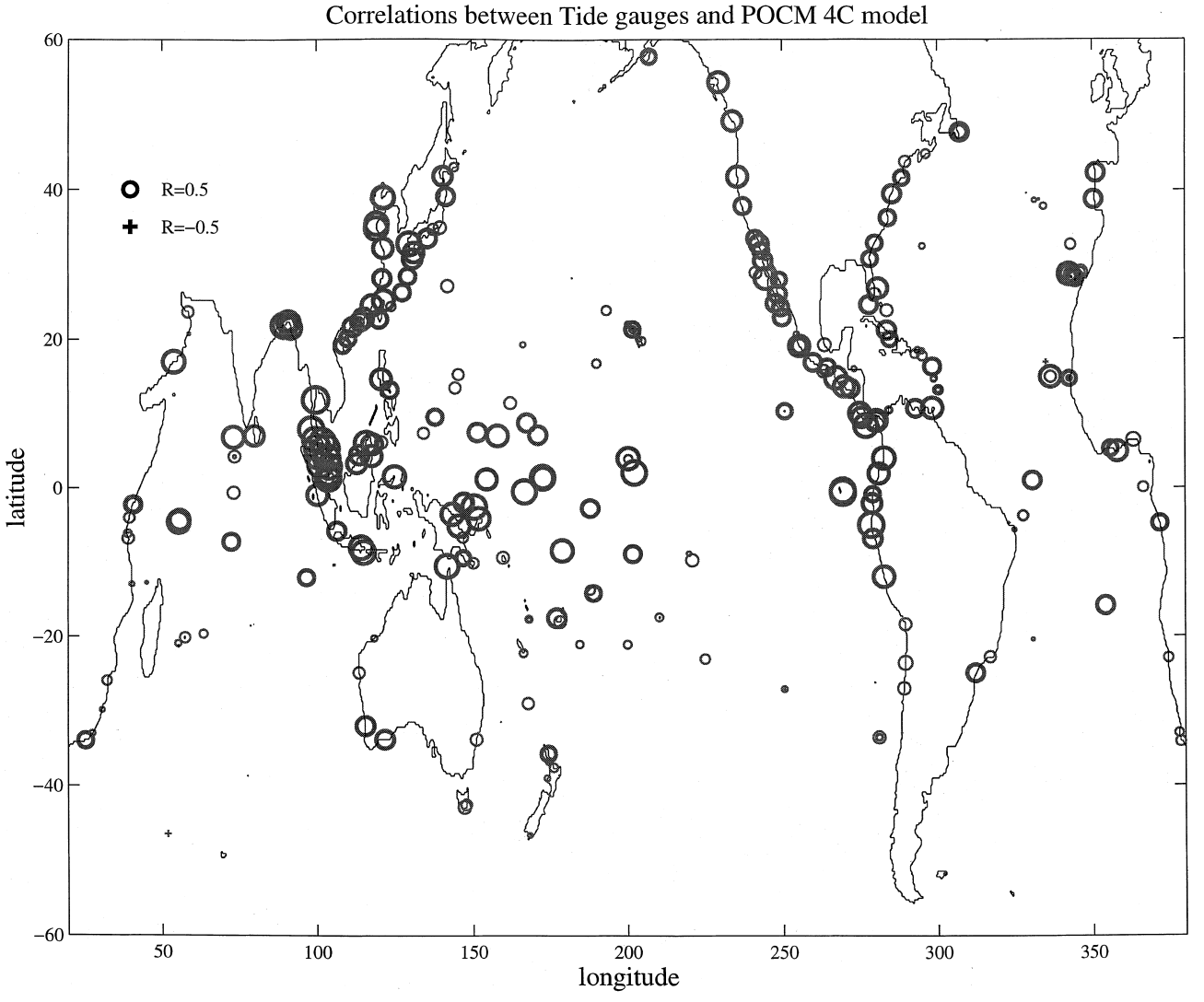

Fig. 3. Correlations between POCM 4C SSH and tide gauges from the University of Hawaii Sea Level Data Center covering the period 1979–1997. Diameter: 1 of circle is proportional to relative correlation value, a cross is relative to size of a negative correlation value.

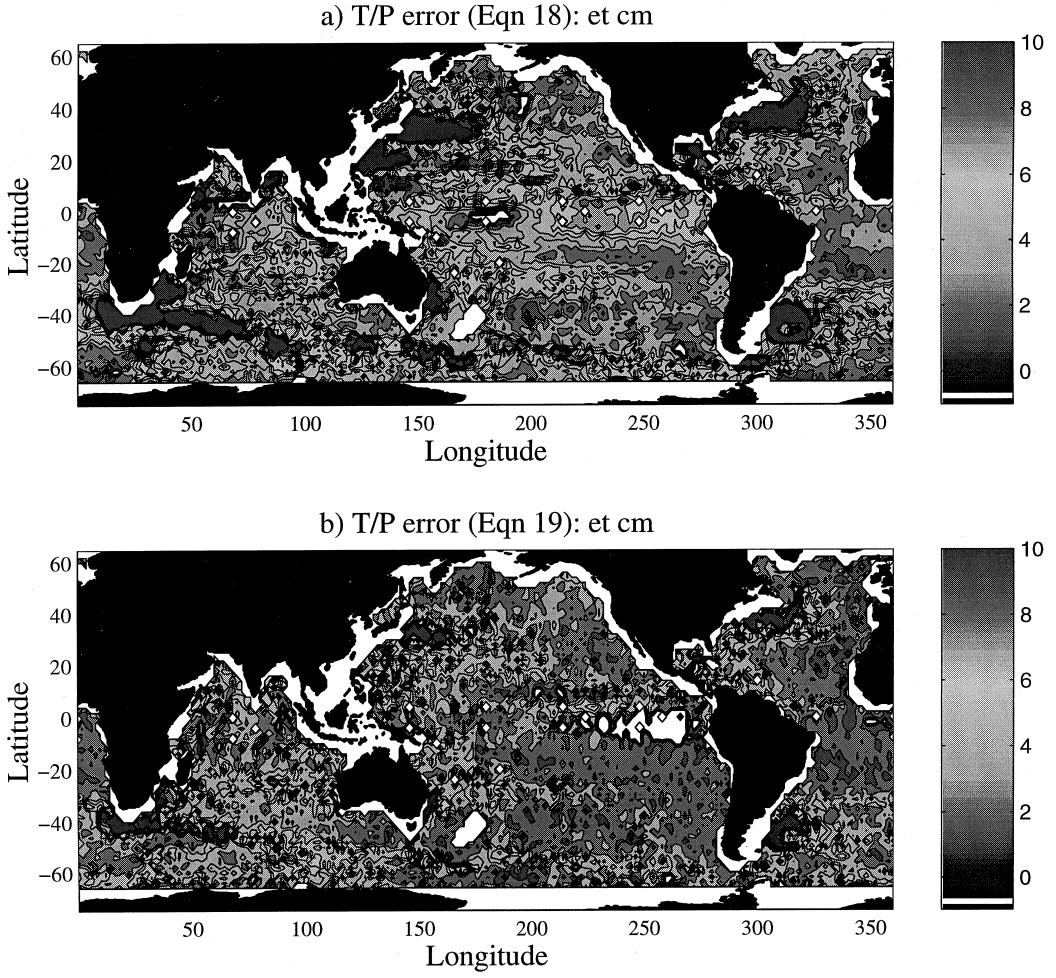

Fig. 4. (a) Estimate of T/P error from Eq. (18), (b) estimate of T/P error from Eq. (19). White denotes a negative estimate.

value. Our best estimate (Eq. (12)) of the true T/P error, *et* is shown in Fig. 2(b). Eq. (18) produces a similar estimate to that computed from Eq. (12) (Fig. 2(b)). The difference between Eqs. (19) and (12) (Fig. 5(a)) is then equal to the quantity: $E(h \cdot ee) - E(h \cdot et)$. Likewise, the difference between Eqs. (18) and (12) (Fig. 5(b)) is $E(h \cdot em) - E(h \cdot et)$. The first difference (Fig. 5(a)) shows that the covariance between *h* and *et* and between *h* and *ee* are either both very similar or both similar and close to zero. We know of no evidence that the error in altimeter measurements is correlated with the sea surface height anomaly. Possible sources of the error would be the inverse barometer correction in the tropics as discussed above, a tidal correction error or an em-bias error. The IB correction in the tropics is small and is not correlated with sea surface height (Fu and Pihos, 1994). In addition, the different sampling characteristics of the two satellites would distort the pattern of any such correlation over the globe. The second explanation seems more likely, i.e. the values are close to zero. Thus, if we accept that $E(h \cdot et)$ is close to zero, most of the difference in

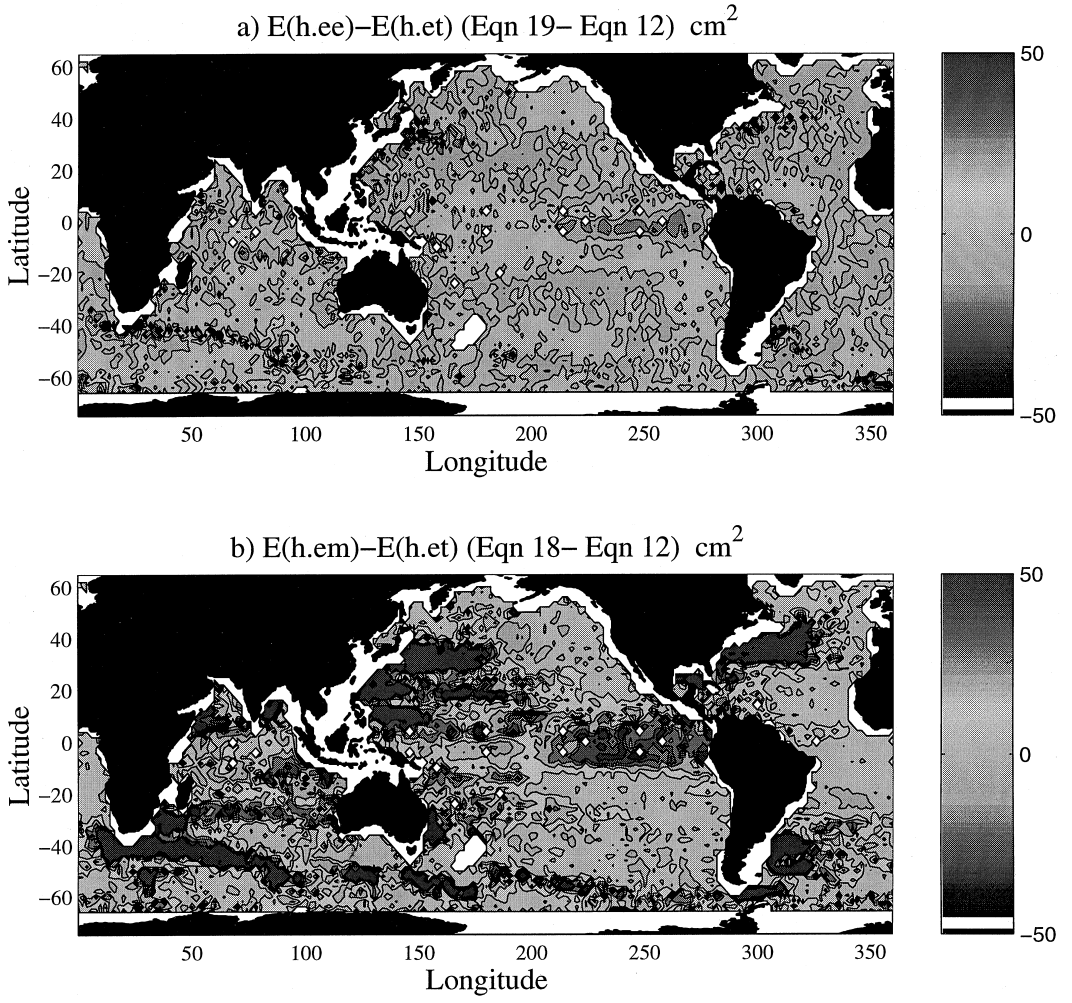

Fig. 5. (a) Difference between error estimated in Eqs. (19) and (12), (b) difference between error estimated in Eqs. (18) and (12).

Fig. 5(b) is attributable to $E(h \cdot em)$. These errors are large (O > 10 cm), larger than the nominal given error of 2–3 cm for Topex and should not be ignored. Thus, through the use of three data sources, a better estimate of the errors, both for the model and the observations can be made.

3.4. Error distributions

In Sections 3.1 and 3.2 we mapped the errors for the two satellite datasets and the model and showed that the error variance is not constant over the globe. In this section, we investigate the relationship between the underlying oceanographic signal and the error variance. Given that the error variance is not constant, the next simplest assumption is that it is proportional to the

underlying signal, i.e. that the error is a constant proportion of the signal. In such a case, a plot of the error variance against the signal on a log scale would show no dependence of the size of the error on the signal amplitude. In our case, we cannot measure the underlying signal, so we use the variance of SSH instead. Fig. 6 shows the log of the error variance plotted against the log of the variance for the model, T/P and ERS-2.

Consider the model first (Fig. 6(a)). There is still a suggestion that the error variance depends on the total variance because the cloud of points is not circular. The global regression coefficient of the log of the error with the log of the variance is 0.99. The coefficients for each 10° of latitude between 0° and 50° are 0.86, 0.99, 1.11, 1.03 and 1.02, respectively. This implies that the error variance is not simply a linear function of the model sea surface height but a more complicated relationship.

Turning now to the satellite data, we see that the distributions are similar (Fig. 6(c) and (e)), except for a line in the ERS-2 plot which corresponds to the high error/variance in the Southern Ocean during the winter months. There are several distinct populations. On the ERS-2 plot (Fig. 6(e)), the red circle identifies the points related to the high error region in the southern ocean. With these points ignored (everything above 50°S along with the corresponding grid locations in the T/P plot, the two plots ((d) and (f)) are quite similar in appearance. Their shape, however, differs from that for the model. In addition to the dense ellipse of points, there is a more diffuse "tail" at the left-hand edge. We suggest that this occurs because there are two parts to the altimeter error signal. The first part is due to instrument error. This is independent of the size of the signal and is responsible for the tail. The mass of points with a structure similar to the model output is caused by sampling error. Here, the error caused by missing energetic features such as eddies or meanders is related to the size of the SSH signal, where SSH is high, eddies etc. are more frequent. For T/P, the global regression coefficient of the log of the error with the log of the variance is 0.60, and, as above, the coefficients for each 10° band are 0.45, 0.56, 0.66, 0.66, and 0.66. ERS 2 data give values of 0.58, globally, and 0.54, 0.56, 0.57, 0.60, and 0.64, for the 10° bands. While both sets of coefficients are similar, the log of the error being about half the log of the variance, there are distinct differences. In the lowest band, 0–10°, the lower T/P value indicates that the variance is less influenced by the total error. If we assume that the instrument error is constant over the globe, then the increase in the coefficient values at the higher latitudes is due to an increase in the sampling error. Since ERS-2's coefficients are lower than T/P's except in the tropical band (0–10°), ERS-2 has a lower sampling error.

4. Conclusions

By combining several instruments' estimates of SSH anomaly, we have shown how a very simplified map of model "error" can be generated for use in assimilation studies. With the assimilation of observational data into a model such as the POCM, the high error regions should be reduced and little change should occur in the low error regions. We have removed a mean field from each of the SSH estimations, thus the bias error (i.e. the difference in the mean circulation) cannot be computed with these data. However, in the future with the incorporation of data from the geodesy missions currently being built (GRACE) or are in the planning stages (CHAMP), we should be able to account for the errors in the model's mean field as well.

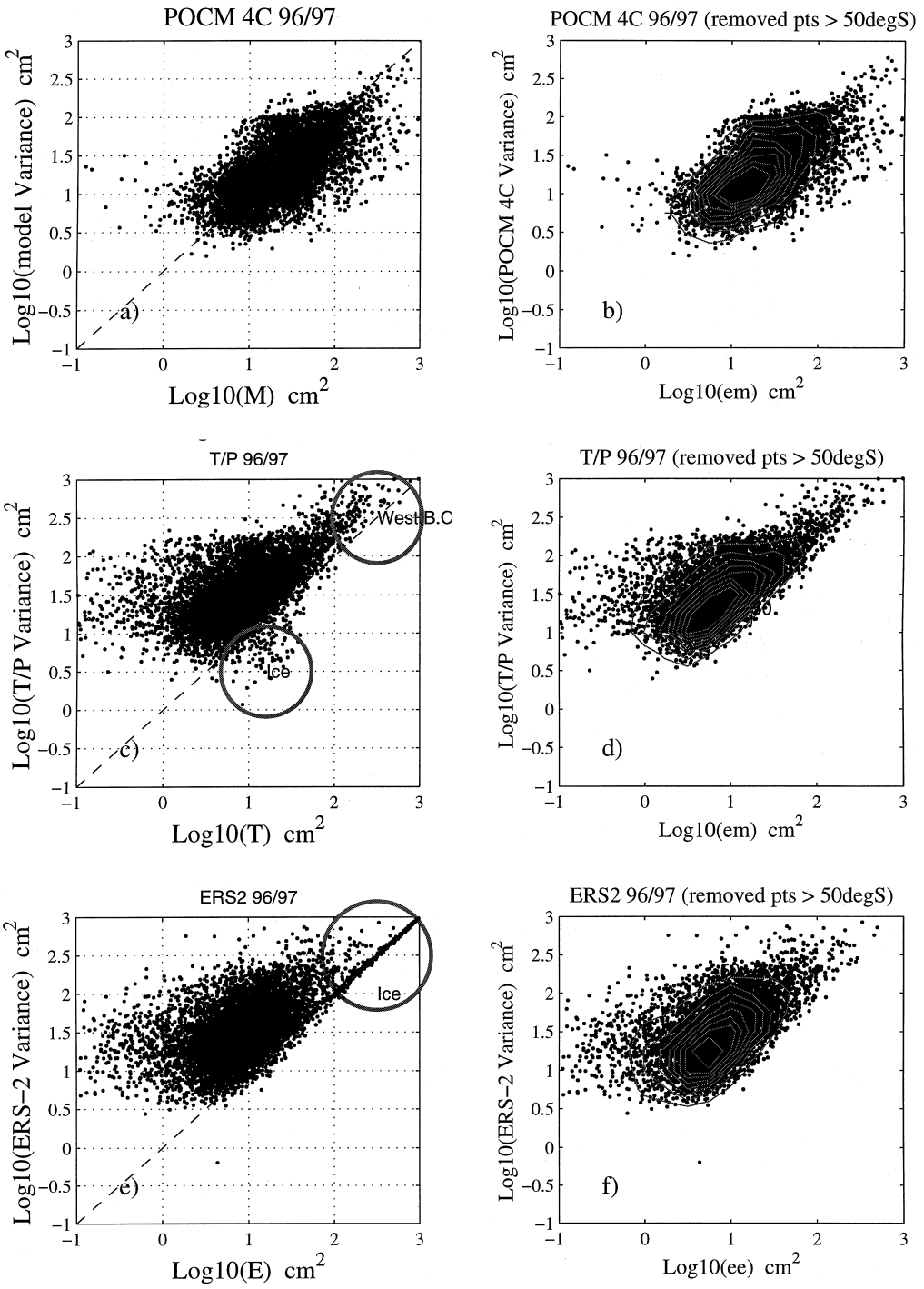

Fig. 6. (a) Log of estimated error versus Log of SSH variance for POCM 4C (b) with points below 50°S removed, contours indicate the density of the points, lines contour the point distribution density every 50 points. (c) Same as (a), but for T/P, (d) same as (b), but for T/P, (e) same as (a), but for ERS-2, (f) same as (b), but for ERS-2.

Acknowledgements

NCAR has provided the computer resources for the model simulation. NASA and the Pathfinder project under C. Koblinsky publicly makes available the satellite data collected by ESA and JPL/CNES. ECMWF provided the wind fields to force the model. This work has been done under a grant of the T/P Extended Mission Science Working Group-JPL Contract no. 960857 (rtt). Thanks to Brian Beckley (GSFC) for creating the special data sets with the em-bias and tidal corrections removed and to the two anonymous reviewers for their time and comments.

References

Bilitza, D., 1997. International reference ionosphere – Status 1995/96. Adv. Space Res. 20, 1751–1754.

Fu, L.L., Pihos, G., 1994. Determining the response of sea level to atmospheric pressure forcing using TOPEX/POSEIDON data. J. Geophys. Res. 99, 24633–24642.

Fukumori, I., 1995. Assimilation of Topex sea level measurements with a reduced-gravity shallow water model of the Tropical Pacific Ocean. J. Geophys. Res. 100, 25027–25039.

Gaspar, P., Ogor, J.P., 1996. Estimation and analysis of the sea state bias of the new ERS-1 and ERS-2 altimetric data (OPR version 6). Technical Report of the IFREMER Contract 96/2.246 002/C.

Hancock III, D.W., Haynes, G.S., 1996. Error in TOPEX Oscillator Drift Correction. topex.wff.nasa.gov/docs/oscdrift.html.

Killworth, P.D., Stainforth, D., Webb, D.J., Paterson, S.M., 1991. The development of a free-surface Bryan–Cox–Semtner ocean model. J. Phys. Oceanogr. 21, 1333–1348.

Kilonsky, B., Caldwell, P., 1991. In the pursuit of high quality SL data. IEEE Oceans Proc. 2, 669–675.

Koblinsky, C., 1998. NASA/GSFC Ocean Pathfinder. neptune.gsfc.nasa.gov/ocean.html.

Marshall, J.A., Zelensky, N.P., Klosko, S.M., Luthcke, S.B., Rachlin, K.E., Williamson, R.G., 1995. The temporal and spatial characteristics of TOPEX/POSEIDON radial orbit error. J. Geophys. Res. 100, 25331–25352.

Scharroo, R., Visser, P., 1998. Precise orbit determination and gravity field improvement for the ERS satellite. J. Geophys. Res. 103, 8113–8128.

Schramma, E.J.O., Ray, R. 1994. A preliminary tidal analysis of Topex/Poseidon altimetry. J. Geophys. Res. 99, 24799–24808.

Semtner, A.J., Chervin, R.M., 1992. Ocean general circulation from a global eddy-resolving model. J. Geophys. Res. 97, 5493–5550.

Stammer, D., Tokmakian, R., Semtner, A.J., Wunsch, C., 1996. How well does 1/4° circulation model simulate large-scale oceanic observations? J. Geophys. Res. 101, 25779–25811.

Tokmakian, R.T., 1996. Comparisons of time series from two global models with tide gauge data. Geophys. Res. Lett. 23, 3759–3762.